scientific reports

Check for updates

OPEN

Control of the near-field radiative heat transfer between graphene-coated nanoparticle metasurfaces

S. G. Castillo-López[1]✉, S. Cortés-López[2] & D. N. Castillo-López[3]

The control of near-field radiative heat transfer (NFRHT) between two metasurfaces can be achieved by manipulating the geometric and dielectric parameters of their components. Based on a 2D effective medium approximation, we describe the dielectric response of each metasurface composed of graphene-coated nanoparticles (GCNPs) on a 2D square lattice as a homogeneous uniaxial film. Wrapping Drude-like nanoparticles (NPs) with graphene enhances the effective plasmonic response of metasurfaces by significantly broadening the frequency range in which surface and hyperbolic waves can be excited by thermal photons. Consequently, the NFRHT between GCNP metasurfaces improves that observed between uncoated Drude-like nanoparticle arrays. We found that the heat flux (Q) grows with increasing metasurface packing fraction (PF) and is also sensitive to GCNP size. By tuning the graphene chemical potential (μ), Q reaches a maximum improvement of 88% for $\mu \approx 0.1$ eV with cores made of Drude-like material, while using cores made of the polar dielectric SiC, Q increases up to 226% for $\mu \approx 0.45$ eV. Our results show that, in addition to the geometric control achieved with uncoated NP arrays, the tunable optical properties of the graphene shell allow dynamic control of the heat flux, expanding the possibilities for NFRHT engineering offered by GCNP metasurfaces.

The radiative heat exchange between two bodies at different temperatures can be successfully described by the well-known Stefan-Boltzmann law when they are separated by a macroscopic vacuum gap, such that the thermal energy is carried only by propagating modes of the electromagnetic field. In the near-field regime, when the distance between the bodies is less than the characteristic thermal wavelength $\lambda_{th} = \hbar c/k_B T$ ($\sim 7.6\ \mu$ m at 300 K), the contribution of the evanescent electromagnetic field to the heat transfer becomes relevant. The near-field radiative heat transfer (NFRHT) between real materials can exceed the predictions of the Stefan-Boltzmann law by several orders of magnitude, as has been demonstrated theoretically and experimentally[1–10]. The protagonism of the evanescent electromagnetic field in the NFRHT makes important the dielectric response of materials since it determines the kind of light-matter interaction that can arise and enhance the heat transfer: surface plasmon polaritons[11–13], surface phonon polaritons[14,15], hyperbolic modes[16,17], epsilon-near-zero (ENZ) modes[18], etc. Then, the management of heat transfer at the nanoscale is possible by tuning the electromagnetic response of the system, for example, by means of external magnetic fields in magneto-optical media[19,20], using phase-change materials such as VO_2[21] or superconductors[22–24], by applying a mechanical strain[25,26], or even using a time-modulated permittivity layer[27].

On the other hand, metasurfaces and metamaterials have been raised as another platform for controlling the NFRHT due to their unusual optical properties shaped by their subwavelength design and the combinations of different dielectric responses of their constituents[28,29]. Metamaterials characterized by periodic subwavelength structures such as multilayers[30], nanowires[31], and nanohole arrays[32] exhibit hyperbolic behavior characterized by super-Planckian thermal radiation in a broad band of the spectrum[16]. Hyperbolic metamaterials also represent an attractive system in which the ENZ properties of electromagnetic modes can be exploited to enhance the NFHRT by a judicious combination of their geometric and dielectric parameters[33]. Metasurfaces made of 2D arrays of spherical nanoparticles (NPs) have also demonstrated their ability to tailor the radiative heat exchange by tuning the effective polaritonic response of the system[34]. Furthermore, for 2D finite ensembles of NPs, the

[1]Instituto de Física, Universidad Nacional Autónoma de México, Apartado Postal 20-364, 01000 Mexico, Mexico. [2]Tecnológico Nacional de México/ ITS de Poza Rica, Luis Donaldo Colosio Murrieta S/N, Arroyo del Maíz, 93230 Poza Rica, Mexico. [3]Facultad de Ciencias de la Electrónica, Benemérita Universidad Autónoma de Puebla, Apartado Postal J-48, 72570 Puebla, Mexico. ✉email: shunashi@fisica.unam.mx

many-body interaction effects on the radiative heat transfer in far and near fields have been studied[35]; and for honeycomb lattices of NPs, topological effects on the radiative heat flux have been demonstrated[36].

Certainly, the electromagnetic response of metasurfaces composed of a monolayer of subwavelength spherical NPs can be reasonably estimated by effective medium approaches (EMAs), such as the anisotropic dipolar model (DM)[37], which is a 2D version of the Maxwell-Garnet model. For a metasurface made of a 2D array of NPs, their effective optical properties, and thus the radiative thermal properties, are determined by several geometrical parameters such as the size, spacing, arrangement, and shape of the NPs, but the composition of the meta-atom also plays an important role. However, a dynamic tunability of the dielectric properties of the metasurface after the fabrication may also be desirable, and this could be possible by including graphene as an element of the meta-atom. Graphene possesses a broadband plasmonic response that can be tuned from the THz to the MIR range by modifying the Fermi level through bias voltage or chemical doping[38]. Using a graphene-coated nanoparticle (GCNP) as a meta-atom of the system significantly modifies the dispersion of the localized polariton mode of individual NPs[39], and consequently, the effective response of the metasurface. GCNP metasurfaces have gained interest due to their outstanding optical properties, such as strong absorption and perfect reflection tunable in deep subwavelength scales[40,41], emerging as single-layer Bragg reflectors. Also, metasurfaces of GCNPs of copper are a useful platform to control plasmon-molecular interactions that enable the nanolasing with lower dye concentrations and with tunable lasing thresholds[42]. On the other hand, arrays of SiC NPs wrapped with graphene have been proposed as a setup for manipulating heat directionality in a many-body system[43]. GCNP arrays can be achieved experimentally by thin-film deposition methods such as chemical vapor deposition[44,45]. Other graphene-based 1D and 2D metasurfaces have also demonstrated interesting near-field optical properties, such as large field enhancement due to the double-resonance effect of plasmonic modes and high quality factor insensitive to the field polarization[46,47]. Also, in the context of NFRHT, periodic arrays of graphene ribbons and patches have exhibited super-Planckian thermal radiation due to the excitation of hyperbolic graphene plasmons[48,49].

In this work, we present a detailed study of the NFRHT between two monolayers of GCNPs arranged in a 2D square lattice. We show that the flexibility offered by the different degrees of freedom of the system allows the passive and active tailoring of the heat flux, which enhances up to 88% using GCNPs with cores made of Drude-like material and up to 226% with cores made of SiC, compared to that observed in arrays of homogeneous NPs.

The paper is organized as follows: In Sect. "2D array of graphene-coated nanoparticles", we provide the theoretical formulation of the problem and the effective dielectric parameters of the system. In Sect. "Results", we present the main results of the NFRHT between metasurfaces, along with a detailed discussion of the results. Finally, in Sect. "Conclusions", we present the conclusions.

2D array of graphene-coated nanoparticles

Our system consists of two identical metasurfaces, each consisting of a 2D square array of graphene-coated spherical nanoparticles on a dielectric substrate. The GCNPs are immersed in a vacuum matrix with permittivity $\varepsilon_M = 1.0$. The dielectric constant of each substrate is $\varepsilon_S = 1.46$. The geometrical parameters of the GCNPs square array are p, the period of the lattice, R, the spherical nanoparticle radius, and w_g, the thickness of the graphene layer. The metasurfaces are placed at different temperatures: $T_1 = 320$ K and $T_2 = 280$ K, and are separated by a vacuum gap of distance L satisfying $L \ll \lambda_{th}$. Both plates are parallel to the x-y plane, as shown in Fig. 1.

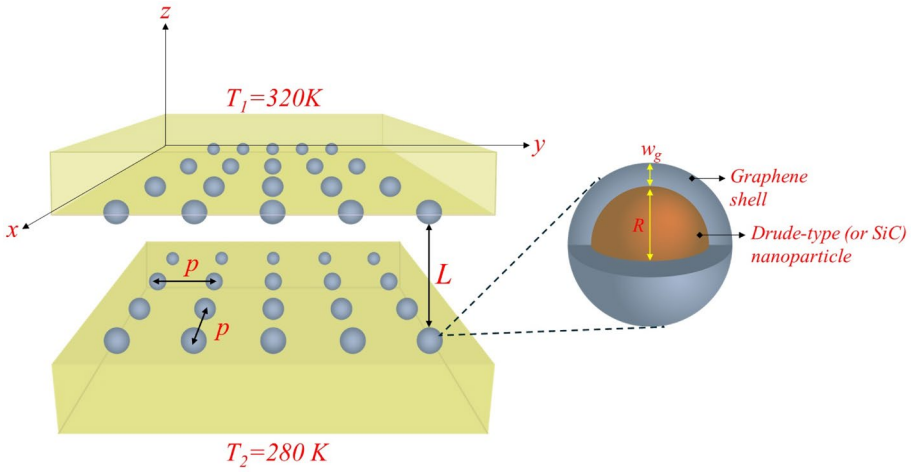

Figure 1. The sketch of the system consists of two metasurfaces, each composed of a monolayer of graphene-coated nanoparticles of radius R arranged in a 2D square lattice with lattice parameter p and supported on a semi-infinite glass substrate with permittivity, $\varepsilon_S = 1.46$. In one case, the nanoparticle cores are composed of a Drude-type material with a plasma frequency in the mid-infrared, and in another case, the cores are made of the polar dielectric SiC. For simplicity, we assume that the nanoparticle arrays are immersed in the vacuum matrix, $\varepsilon_M = 1.0$. The metasurfaces are at different temperatures $T_1 = 320$ K and $T_2 = 280$ K and separated by a vacuum gap $L = 50$ nm.

The electromagnetic response of the nanoparticle core is of Drude type, with a frequency-dependent permittivity $\varepsilon_c(\omega) = 1 - \omega_p^2/(\omega^2 + i\omega\nu)$, where ω is the frequency, ω_p is the plasma frequency of free charge carriers, and $\nu = 0.01\ \omega_p$ is the damping parameter. For our calculations, we choose the plasma frequency, $\omega_p = 1 \times 10^{14}$ rad/s, which lies in the frequency range of the infrared spectrum and corresponds to a doped semiconductor material. When dealing with NPs containing polar dielectric cores, we use SiC, which has a dielectric function given by $\varepsilon_{SiC}(\omega) = \varepsilon_\infty(\omega^2 - \omega_{LO}^2 + i\gamma\omega)/(\omega^2 - \omega_{TO}^2 + i\gamma\omega)$, where $\varepsilon_\infty = 6.7$, $\omega_{LO} = 1.825 \times 10^{14}$ rad/s, $\omega_{TO} = 1.494 \times 10^{14}$ rad/s, and $\gamma = 8.966 \times 10^{11}$ rad/s[50]. We selected these two core materials because the resonance frequency of the localized mode of individual nanoparticles can be excited by mid-infrared thermal photons. A comprehensive analysis of how the variation of the dielectric parameters associated with two core-shell NPs affects the NFRHT is detailed in Ref.[51] in terms of surface modes hybridization. The material of the nanoparticle shell is a 2D graphene monolayer, which can be regarded as an ultra-thin material of thickness $w_g = 0.334$ nm with optical properties described by the equivalent dielectric function $\varepsilon_g(\omega) = 1 + i\sigma_g(\omega)/(\varepsilon_0\omega w_g)$, where ϵ_0 is the vacuum permittivity and σ_g is the frequency-dependent graphene conductivity[38,52]. Based on the Kubo formula, the graphene conductivity can be calculated as $\sigma_g(\omega) = \sigma_{intra}(\omega) + \sigma_{inter}(\omega)$, with

$$\sigma_{intra}(\omega) = \frac{2ie^2 k_B T}{\pi\hbar^2(\omega + i\tau^{-1})} \log\left[2\cosh\left(\frac{\mu}{2k_B T}\right)\right], \tag{1a}$$

$$\sigma_{inter}(\omega) = \frac{e^2}{4\hbar}\left\{\frac{1}{2} + \frac{1}{\pi}\arctan\left[\frac{\hbar\omega - 2\mu}{2k_B T}\right] - \frac{i}{2\pi}\log\frac{(\hbar\omega + 2\mu)^2}{(\hbar\omega - 2\mu)^2 + (2k_B T)^2}\right\}, \tag{1b}$$

where e is the electron charge, k_B is the Boltzmann constant, T is the temperature, τ is the carrier relaxation lifetime, and μ is the chemical potential, which can be modified with external stimuli, e.g. by vias voltage or chemical doping. In these expressions, $\sigma_{intra}(\omega)$ and $\sigma_{inter}(\omega)$ take into account the intraband electron-photon scattering processes and the direct interband electron transitions, respectively.

The dielectric response of each GCNP array is effectively described by the DM, which is based on quasi-static and mean-field approximations[34]. The DM considers only the dipolar contributions to the electromagnetic response of the nanoparticles, taking into account the dipole-dipole interactions between real nanoparticles and the interactions between the induced dipoles in the nanoparticles and their image dipoles induced in the substrate. The DM assumptions are valid in the quasi-static limit, as in many other EMAs. In our case, this scenario is guaranteed by satisfying the conditions $R < p \ll \lambda_{th}$ and $L > p/2\pi$[32], with the dominant wavelength of thermal photons of the micron size being much larger than the characteristic lengths of the system. According to DM, the components of the effective permittivity tensor, $\overleftrightarrow{\varepsilon} = diag(\varepsilon_\parallel, \varepsilon_\parallel, \varepsilon_\perp)$, of each anisotropic metasurface, are given by:

$$\varepsilon_{||} = \left[1 + \frac{2\pi(R/p)^2\tilde{\alpha}}{1 - A\tilde{\alpha}/8 - (R/p)^3(\xi_0 + A\xi_I)\tilde{\alpha}/2}\right]\varepsilon_M, \quad \text{and} \quad \varepsilon_\perp = \left[1 - \frac{2\pi(R/p)^2\tilde{\alpha}}{1 - A\tilde{\alpha}/4 + (R/p)^3(\xi_0 - A\xi_I)\tilde{\alpha}}\right]^{-1}\varepsilon_M, \tag{2}$$

where $A = (\varepsilon_S - \varepsilon_M)/(\varepsilon_S + \varepsilon_M)$ is the image charge factor,

$\tilde{\alpha}$ is the normalized polarizability of individual core-shell nanoparticle[53],

$$\tilde{\alpha} = \frac{(\varepsilon_g - \varepsilon_M)(\varepsilon_c + 2\varepsilon_g) + \left[(R - w_g)/R\right]^3(\varepsilon_c - \varepsilon_g)(2\varepsilon_g + \varepsilon_M)}{(\varepsilon_g + 2\varepsilon_M)(\varepsilon_c + 2\varepsilon_g) + \left[(R - w_g)/R\right]^3(\varepsilon_c - \varepsilon_g)(2\varepsilon_g - 2\varepsilon_M)}, \tag{3}$$

and ξ_0 and ξ_I are sums over the number of nanoparticles along both x and y directions, defined as,

$$\xi_0 = \sum_{n,m=-\infty}^{\infty}\frac{1}{(n^2 + m^2)^{3/2}} = 0.90336, \qquad \xi_I = \sum_{n,m=-\infty}^{\infty}\frac{3(2R/p)^2 - (n^2 + m^2 + (2R/p)^2)}{\left[n^2 + m^2 + (2R/p)^2\right]^{5/2}}. \tag{4}$$

To go further, we based the study of the NFRHT between two parallel metasurfaces on the expressions derived within the framework of Rytov's theory of fluctuating electrodynamics[1,2], where the total heat flux is obtained as $Q = \int_0^\infty d\omega\, S(\omega)$, being the spectral flux:

$$S(\omega) = [\Theta(\omega, T_1) - \Theta(\omega, T_2)]\sum_{i=p,s}\int\frac{d\kappa\kappa}{(2\pi)^2}\left[\mathscr{T}_i^{\text{prop}}(\omega, \kappa) + \mathscr{T}_i^{\text{evan}}(\omega, \kappa)\right]. \tag{5}$$

Here, $\Theta(\omega, T) = \hbar\omega/\left[\exp(\hbar\omega/k_B T) - 1\right]$ is the average energy of thermal harmonic oscillators, and κ corresponds to the magnitude of the wavevector in the $x - y$ plane. The sum in Eq. (5) considers the contribution of p- and s-polarized waves of the propagating ($\kappa < \omega/c$) and evanescent ($\kappa > \omega/c$) fields through the energy transmission coefficients $\mathscr{T}_{i=p,s}^{\text{prop}}$, and $\mathscr{T}_{i=p,s}^{\text{evan}}$, given by the expressions,

$$\mathscr{T}_{i=p,s}^{\text{prop}}(\omega, \kappa, L) = \frac{\left(1 - |r^i|^2\right)^2}{|1 - (r^i)^2\exp(2ik_z L)|^2}, \qquad \mathscr{T}_{i=p,s}^{\text{evan}}(\omega, \kappa, L) = \frac{4\left[\text{Im}\,(r^i)\right]^2\exp(-2|k_z|L)}{|1 - (r^i)^2\exp(-2|k_z|L)|^2}, \tag{6}$$

where k_z represents the component of the wavevector along the z direction. The reflection coefficients associated with the entire metasurface, r^i, can be calculated as detailed in the Supplementary Information (SI).

Results

We study the NFRHT between two identical metasurfaces made of GCNPs arranged in a 2D square lattice, which are placed at different temperatures $T_1 = 320$ K and $T_2 = 280$ K, and separated by a vacuum gap $L = 50$ nm. Unless otherwise indicated, we use in the following calculations $\mu = 0.15$ eV. The total heat flux, Q, as a function of nanoparticle radius, R, and packing fraction (PF), defined as the ratio PF$\equiv R/p$, is shown as the multicolor surface in Fig. 2. As expected, Q grows with increasing PF for all particle sizes since a denser packing favors the coupling of the nanoparticle modes and thus, the excitation of new lattice modes[34]. On the other hand, the increment of Q with increasing nanoparticle radius while the PF is fixed is a less obvious result that we observed. This unexpected behavior shows that, in this case, the GCNP size itself is relevant in shaping the radiative heat transfer, as we will discuss below. Comparison with the case of metasurfaces made of uncoated homogeneous NPs (green surface) shows an enhancement of Q when the NPs are covered with graphene. The relative change $(Q_{GCNP}/Q_{HNP} - 1) \times 100$ of the heat flux between two GCNP metasurfaces (Q_{GCNP}) with respect to that obtained between two homogeneous NP arrays (Q_{HNP}) is shown using the color scale indicated by the bar legend. We predict that the heat flux between metasurfaces increases up to 76% for the case of GCNPs with the maximum packing PF $= 0.5$.

In order to clarify the effect of the NP radius in the heat transfer between metasurfaces, we present in Fig. 3 contour plots of each surface shown previously in Fig. 2. White contours in the plots depict constant values of Q. Figure 3a reveals that the heat exchanged between metasurfaces of homogeneous NPs does not change with the NP radius for small values of the PF $\lesssim 0.36$, i.e. Q only depends on the PF. As the array packing becomes denser, a slight dependence on the radius is observed. On the other hand, when NPs are coated with graphene, the heat flux between metasurfaces becomes very sensitive to the NP size. Also, notice that the heat flux between metasurfaces increases with R for the case of GCNPs, while for homogeneous NPs with dense packing, the maximum Q is reached with small particles. Even when the metasurface is described as a homogeneous anisotropic medium with effective dielectric properties derived from an EMA, the reason for the sensitivity of the NFRHT to the NP size can be understood by observing the explicit R dependence of the nanoparticle polarizability (3) for a core-shell configuration. The resonance condition, $\tilde{\alpha} \to \infty$, to excite surface modes in each nanoparticle can be modified by varying the radius and also by changing the dielectric properties of the shell[54]. Then, the radius not only affects the NFRHT as a geometrical parameter that tunes the hybridization of each NP mode throughout the whole lattice via the PF, but also shapes the plasmonic response of individual GCNP. As a result, the increasing of GCNP size redshifts the resonance frequency of its localized surface modes, making them more accessible to thermal photons, while for homogeneous nanoparticles, the localized surface plasmon resonance always occurs at $\omega \sim \omega_p/\sqrt{3}$ independent of the NP radius.

Interestingly, graphene coating also modifies the local density of electromagnetic modes in the cavity between the two metasurfaces and thus the spectral energy density $S(\omega)$. In Fig. 4, we present $S(\omega)$ as a function of normalized frequency ω/ω_0 and the nanoparticle size for the case of metasurfaces composed by GCNPs (a) and homogeneous NPs (b). Here $\omega_0 = 10^{14}$ rad /s. Because the NP array behaves as an effective uniaxial material

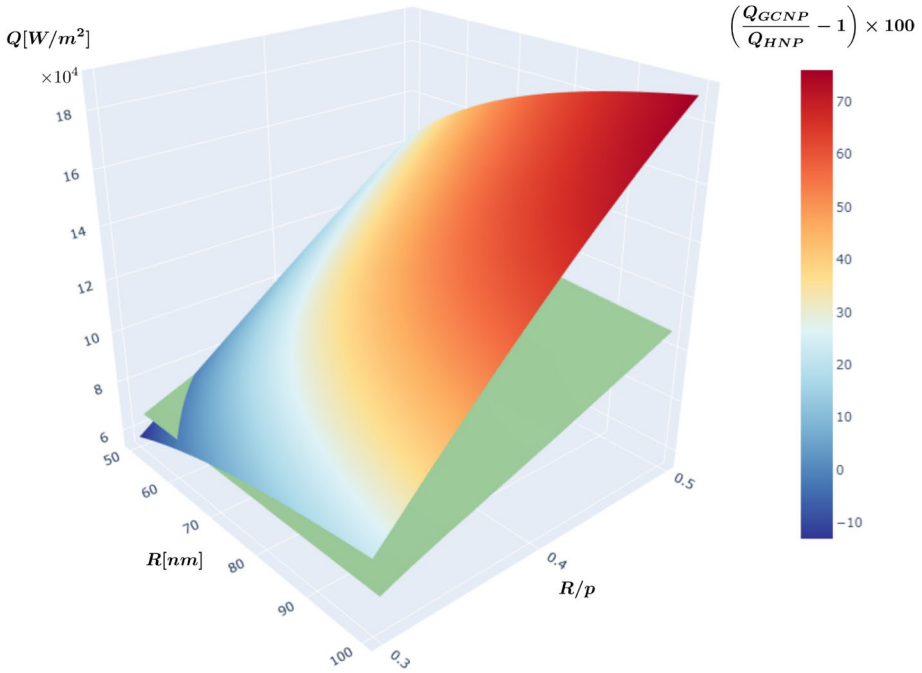

Figure 2. Total heat flux, Q, between 2D ordered arrays of GCNPs (multicolored surface) and homogeneous NPs (green surface) as a function of nanoparticle radius, R, and packing fraction, R/p. The color scale indicated by the legend bar corresponds to a comparison of the heat flux exchanged by the nanoparticle arrays with and without graphene coating. Here $\mu = 0.15$ eV.

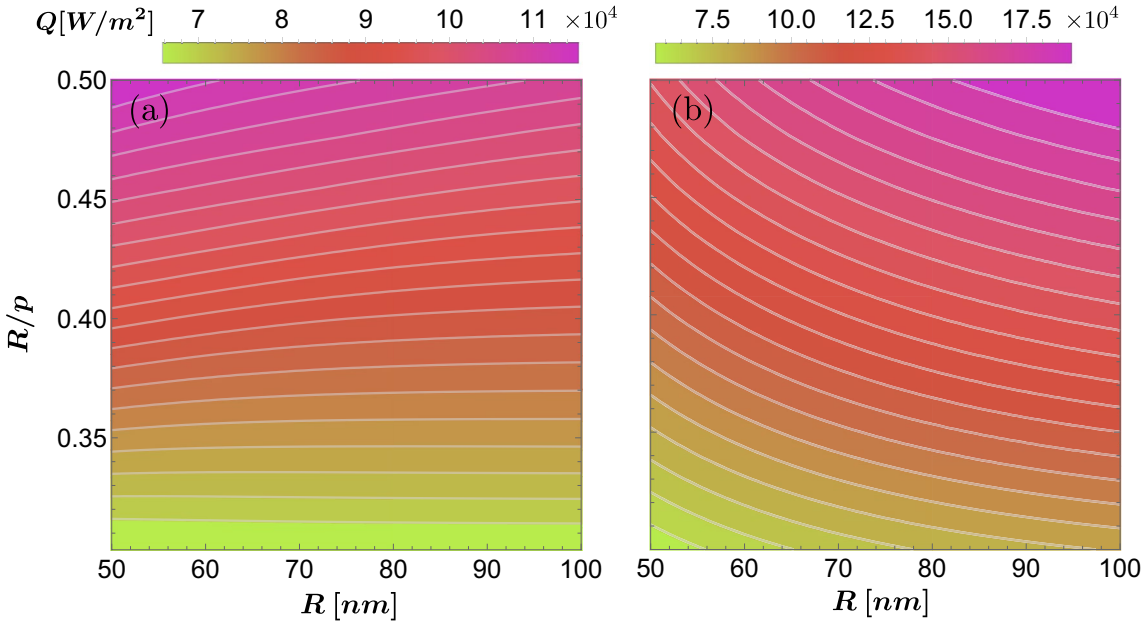

Figure 3. Contour plots of the total heat flux surfaces shown in Fig. 2. Here (**a**) corresponds to the case of 2D ordered arrays of homogeneous NPs and (**b**) corresponds to GCNP metasurfaces. Each contour represents curves of constant Q.

under the conditions we consider, two kinds of modes can contribute to the heat flux: surface (SWs) and hyperbolic (HWs) waves, which can be excited on frequency range where Re $\varepsilon_\perp < 0$, Re $\varepsilon_\parallel < 0$ and Re $\varepsilon_\perp \gtrless 0$, Re $\varepsilon_\parallel \lesseqgtr 0$, respectively. Comparison of (a) and (b) reveals that the regions where SWs and HWs can be excited widen when the NPs are coated with graphene. Also, for the arrays of GCNPs, the maxima of $S(\omega)$ move to lower frequencies with increasing R, consistent with the redshift of the resonance frequency of individual NPs. On the other hand, for the arrays of homogeneous NPs, the maximum values of $S(\omega)$ practically do not change with R, except for small radii where two maxima are distinguished in low frequency range, but they overlap in frequency as R increases. This is probably due to the fact that the effective width of the nanoparticle layer increases with R, decoupling the surface modes of the outermost interfaces. In Fig. 4c and d, we plot the spectral heat flux dependence on the packing fraction PF for GCNP metasurfaces and homogeneous NP arrays, respectively. In both cases, our observations suggest a broadening of the SWs frequency region with increasing PF, accompanied by a narrowing of the HWs region. This predicts an isotropic response of the metasurfaces around PF ~ 0.47. Furthermore, we found that GCNP metasurfaces allow the excitation of SWs and HWs in significantly wider frequency ranges for all PF values (compare (c) and (d)). Note that in the limit of low PF when the separation between NPs inhibits the coupling of its plasmonic modes through the whole array, the heat flux is spectrally localized around the surface plasmon resonance of a single NP at $\omega/\omega_0 \approx 0.58$ and $\omega/\omega_0 \approx 1.24$ for homogeneous and graphene-coated nanoparticles, respectively.

GCNP metasurfaces sustained modes

The effect of the graphene coating on the dispersion of the modes sustained by the cavity is illustrated by comparing the energy transmission coefficient $\mathcal{T}_p(\omega, \kappa)$ between metasurfaces made of GCNPs and homogeneous NPs in Fig. 5a and b, respectively. Here we plot $\mathcal{T}_p(\omega, \kappa)$ as a function of the normalized in-plane wavevector $\kappa c/\omega$ and the frequency ω/ω_0 for the parameters $R = 100$ nm and PF $= 1/3$. Since we consider the NP core made of a Drude-like material, the graphene coating does not induce the appearance of new plasmonic modes as it does for cores made of polar dielectrics[39]. Instead, the graphene shell notably modifies the dispersion of the already present modes: it duplicates the frequency windows where HWs (shaded regions) and SWs (the band in between) can be excited and broadens the linewidth of all these modes. The latter is a consequence of the increased damping of the modes, which is also reflected in the reduction of their maximum value of the in-plane wave vector. On the other hand, a part of the upper branch of the symmetric SWs and a partial region of HWs fall into a frequency range where the $\varepsilon_\perp$ component displays an ENZ behavior[55]. This ENZ behavior means that these modes exhibit a strong enhancement of the electric field along the z-direction. The intensity of this enhancement is quantified by the factor $k_{ENZ} = |\varepsilon_\perp|^{-2}$. The white dotted area in Fig. 5a,b corresponds to the ENZ region where $k_{ENZ} > 20$. Using GCNPs in metasurfaces to enhance plasmonic properties entails an increase in the material losses, which reduces the ENZ character of SWs and HWs by two orders of magnitude, since $k_{ENZ} \sim |\text{Im } \varepsilon_\perp|^{-2}$. However, because of the resonant nature of SWs, the hybridization of such modes provides the principal contribution to the NFRHT between metasurfaces, even as the ENZ character decreases and the contribution of HWs becomes less relevant. Since the ENZ regions depend on the anisotropy of the medium[56], the frequency range where the metasurface exhibits an ENZ behavior notably changes with the packaging fraction, blue shifting with increasing relation R/p as the dotted region in Fig. 4c,d shows. Details of the dielectric response of the metasurface and the k_{ENZ} factor for the cases presented above are given in the SI.

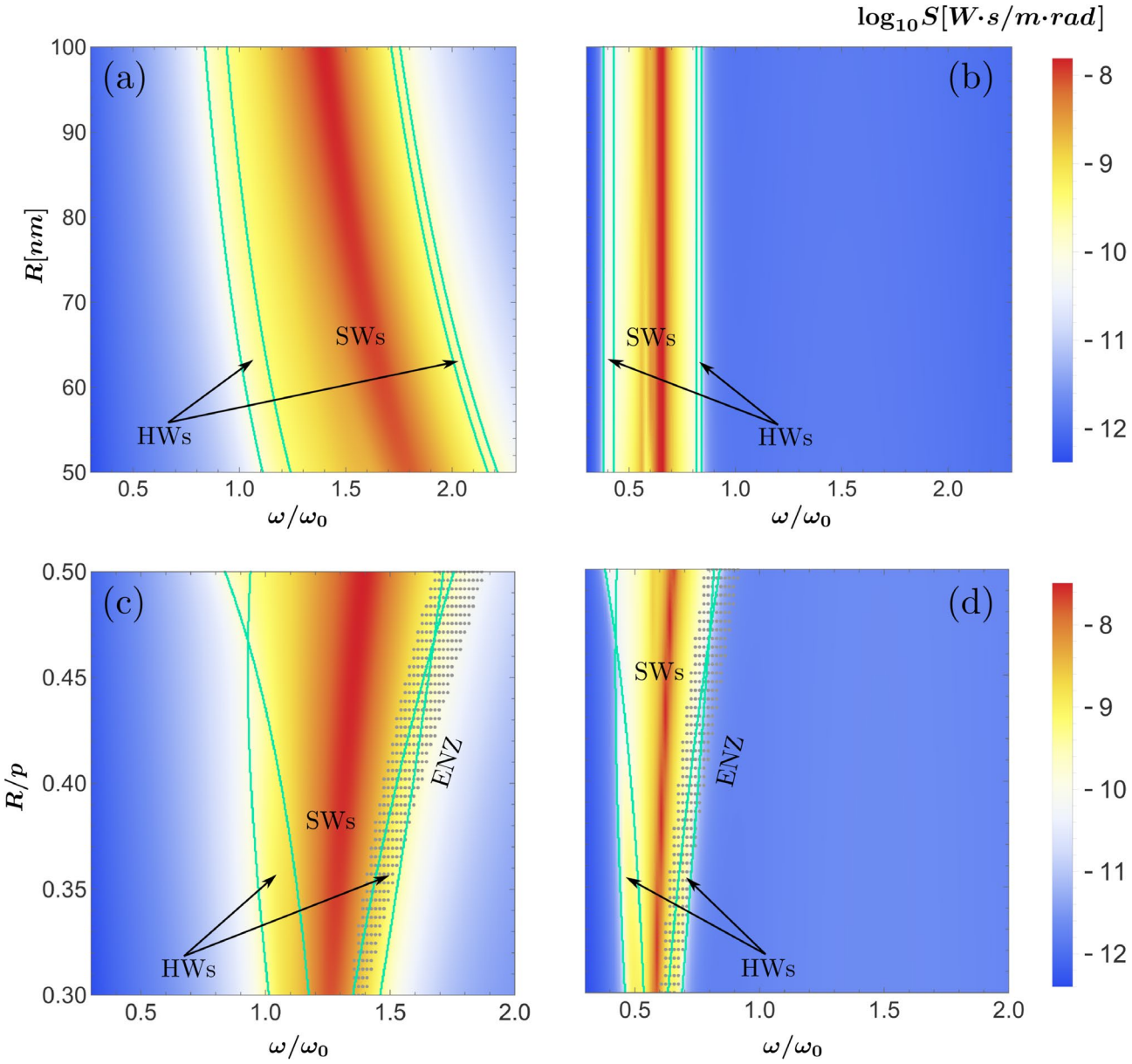

Figure 4. Spectral heat flux S as a function of the normalized frequency ω/ω_0 and NP radius R, (**a**) and (**b**), packing fraction R/p, (**c**) and (**d**), between two metasurfaces made of GCNPs and homogeneous NPs, respectively. In figures (**a**,**b**) PF $= 0.5$, in (**c**,**d**) $R = 100$ nm, and in figures (**a**,**c**) $\mu = 0.15$ eV.

Moreover, the use of graphene as the coating material of NPs provides an additional degree of freedom for tailoring the heat transfer in the system by tuning the graphene permittivity ε_g through the chemical potential μ. Figure 6 shows the effect of μ on the total heat flux between the metasurfaces of GCNPs. When the core of the GCNP is made of a plasmonic material with a dielectric response given by the Drude model, the heat flux between GCNP metasurfaces (red dots) exceeds that observed between two homogeneous NP arrays (horizontal red line), increasing up to 88% for low values of the chemical potential $\mu < 0.35$ eV. The upper inset images show the $\mathcal{T}_p$ coefficients of the system composed of homogeneous NPs (left) and GCNPs (right) with a Drude-like core. The latter was calculated using the optimal value $\mu = 0.1$ eV associated with the maximum value of Q shown by purple dots. The graphene coating broadens the frequency range in which the different modes of the system can be excited, thereby increasing the heat flux of the system. As expected, with further increasing μ, the SW and HWS regions move to higher frequencies and become less accessible to thermal photons, causing Q to drop below the heat flux obtained with homogeneous NPs. On the other hand, for GCNPs with cores made of the polar dielectric SiC (blue dots), Q increases more than 226% by about $\mu \approx 0.45$ eV compared to the heat flux obtained between homogeneous NP arrays and continues to exceed it even for higher values of μ. The lower images of the inset compare the $\mathcal{T}_p$ coefficients between two arrays of SiC NPs with (right) and without (left) graphene coating. For polar dielectric NPs, the graphene coating not only widens the frequency window of the surface modes of

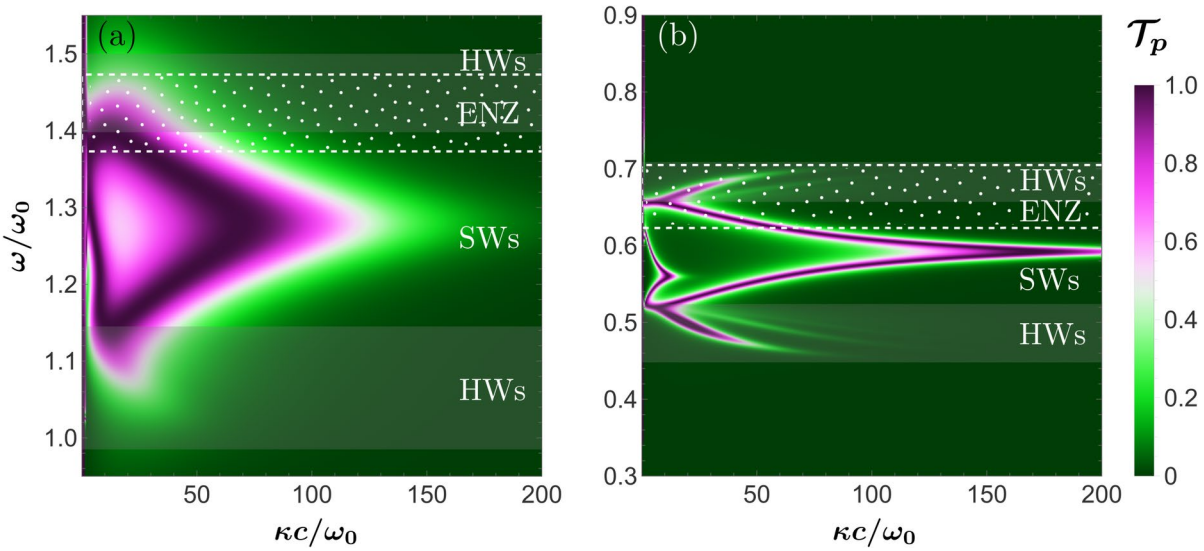

Figure 5. The energy transmission coefficient of p-polarized waves as a function of the normalized frequency ω/ω_0 and the parallel wave vector $\kappa c/\omega_0$ for the system composed of two GCNPs arrays (**a**) and homogeneous NPs arrays (**b**). In both figures $R = 100$ nm and PF $= 1/3$, and in figure (**a**), $\mu = 0.15$ eV.

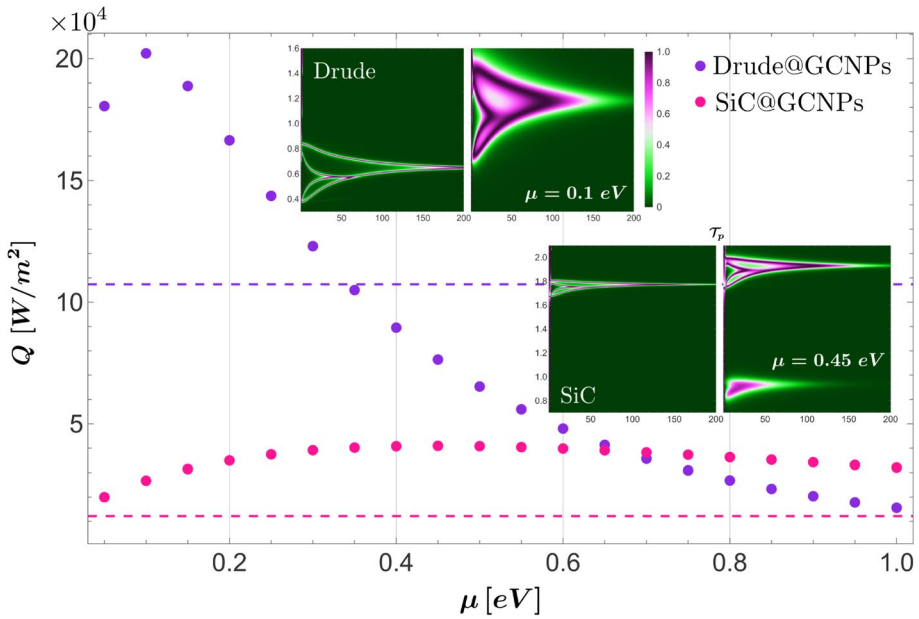

Figure 6. Total heat flux, Q, between GCNP metasurfaces as a function of the chemical potential of the graphene coating, μ. Purple (pink) dots correspond to GCNPS with cores made of Drude-like material (SiC), while the dashed horizontal line depicts that value of Q calculated for the corresponding homogeneous NP array. The inset of the figure shows the $\mathcal{T}_p$ coefficient as a function of the normalized frequency ω/ω_0 and the longitudinal wavevector $\kappa/c\omega_0$. In the top (bottom) plots we show the results for two metasurfaces made of Drude-like (SiC) NPs, with the case of homogeneous NPs on the left and the case of GCNPS on the right. In all calculations, PF $= 0.5$ and $R = 100$ nm.

the metasurfaces but also leads to the presence of new plasmonic modes at low frequencies[43], which improves the NFRHT of the system compared to homogeneous NP arrays for a wide range of chemical potential values.

Tuning the spectrum of the NFRHT using an extended variety of hyperbolic metamaterials has been investigated with array structures of multilayers, nanopillars, nanoholes, nanoparticles, etc. through the geometrical design[34,57], however, including graphene as a part of the system also allows the active control of the NFRHT after fabrication. The heat flux between periodic arrays of graphene nanoribbons or nanopatches can be tailored by varying the filling fraction, lattice parameter, and also the chemical potential of graphene[48,49]. Comparison of these graphene-based metasurfaces with the GCNP metasurfaces presented in this work shows maximum spectral heat flux values an order of magnitude higher for the latter. Also, notice that GCNPs provide an extra

degree of freedom associated with the dielectric parameters of the core material, which could play an important role in improving heat transfer.

Conclusions

We show in this work that metasurfaces consisting of a substrate decorated with graphene-coated nanoparticles offer additional possibilities to control NFRHT. In particular, the heat flux between two identical metasurfaces of this kind becomes more sensitive to the nanoparticle radius compared to the heat flux between metasurfaces made of homogeneous nanoparticles. Due to the effect of the graphene coating, the increase of the nanoparticle radius will not only act as a geometrical parameter tuning the hybridization of the modes of each NP through the whole lattice but it will also redshift the resonance frequency of its localized surface modes, making them more accessible to thermal photons. This effect is unveiled by spectral analysis of the heat flux, which also shows a significant broadening of the frequency range where the modes sustained by the cavity can be excited. In addition, using graphene as a coating material for the NPs provides an extra degree of freedom for tailoring the heat transfer in the system by tuning the graphene permittivity via its chemical potential, achieving an appreciable enhancement of the NFRHT. The tunable optical properties enabled by coating the nanoparticles with graphene offer the possibility of obtaining dynamical metasurfaces capable of active control of NFRHT and widen the perspectives of heat transfer engineering. This also contributes to efforts to study metasurfaces for the development of optical, electronic, photonic, and optoelectronic devices with tunable optical, electrical, or thermal properties.

Data availibility

The datasets used and/or analysed during the current study available from the corresponding author on reasonable request.

Received: 31 May 2024; Accepted: 30 July 2024
Published online: 07 August 2024

References

1. Polder, D. & Van Hove, M. Theory of radiative heat transfer between closely spaced bodies. *Phys. Rev. B* **4**, 3303–3314 (1971).
2. Vinogradov, E. A. & Dorofeev, I. A. Thermally stimulated electromagnetic fields of solids. *Phys.-Usp.* **52**, 425 (2009).
3. Pascale, M., Giteau, M. & Papadakis, G. T. Perspective on near-field radiative heat transfer. *Appl. Phys. Lett.* **122**, 100501 (2023).
4. Pérez-Rodríguez, J., Pirruccio, G. & Esquivel-Sirvent, R. Spectral gaps in the near-field heat flux. *Phys. Rev. Mater.* **3**, 015201 (2019).
5. Biehs, S.-A. *et al.* Near-field radiative heat transfer in many-body systems. *Rev. Mod. Phys.* **93**, 025009 (2021).
6. De Wilde, Y. *et al.* Thermal radiation scanning tunnelling microscopy. *Nature* **444**, 740–743 (2006).
7. Kittel, A. *et al.* Near-field heat transfer in a scanning thermal microscope. *Phys. Rev. Lett.* **95**, 224301 (2005).
8. Shen, S., Narayanaswamy, A. & Chen, G. Surface phonon polaritons mediated energy transfer between nanoscale gaps. *Nano Lett.* **9**, 2909–2913 (2009).
9. St-Gelais, R., Guha, B., Zhu, L., Fan, S. & Lipson, M. Demonstration of strong near-field radiative heat transfer between integrated nanostructures. *Nano Lett.* **14**, 6971–6975 (2014).
10. Francoeur, M. Near-field radiative energy transfer: Nanostructures feel the heat. *Nat. Nanotechnol.* **10**, 206–208 (2015).
11. Wang, L. *et al.* Giant near-field radiative heat transfer between ultrathin metallic films. *Opt. Express* **27**, 36790–36798 (2019).
12. Xu, D., Zhao, J. & Liu, L. Photon tunneling mechanism of internal plasmon polaritons between two thick slabs under near-field radiation excitation. *J. Quant. Spectrosc. Radiat. Transf.* **314**, 108855 (2024).
13. Su, C. & Fu, C. Near-field radiative heat transfer between two α-quartz plates having hyperbolic and double-negative-permittivity bands. *Int. J. Heat Mass Transf.* **196**, 123235. https://doi.org/10.1016/j.ijheatmasstransfer.2022.123235 (2022).
14. Francoeur, M., Mengüç, M. P. & Vaillon, R. Near-field radiative heat transfer enhancement via surface phonon polaritons coupling in thin films. *Appl. Phys. Lett.* **93**, 043109-1–0431093-3 (2008).
15. Song, B. *et al.* Enhancement of near-field radiative heat transfer using polar dielectric thin films. *Nat. Nanotechnol.* **10**, 253–258 (2015).
16. Biehs, S.-A., Tschikin, M. & Ben-Abdallah, P. Hyperbolic metamaterials as an analog of a blackbody in the near field. *Phys. Rev. Lett.* **109**, 104301 (2012).
17. Liu, R., Ge, L., Wu, B., Cui, Z. & Wu, X. Near-field radiative heat transfer between topological insulators via surface plasmon polaritons. *iScience* **24**, 103408 (2021).
18. Hajian, H., Rukhlenko, I. D., Erçağlar, V., Hanson, G. & Ozbay, E. Epsilon-near-zero enhancement of near-field radiative heat transfer in bp/hbn and bp/α-moo3 parallel-plate structures. *Appl. Phys. Lett.* **120**, 112204 (2022).
19. Moncada-Villa, E., Fernández-Hurtado, V., Garcia-Vidal, F. J., García-Martín, A. & Cuevas, J. C. Magnetic field control of near-field radiative heat transfer and the realization of highly tunable hyperbolic thermal emitters. *Phys. Rev. B* **92**, 125418 (2015).
20. Castillo-López, S., Márquez, A. & Esquivel-Sirvent, R. Resonant enhancement of the near-field radiative heat transfer in nanoparticles. *Phys. Rev. B* **105**, 155404 (2022).
21. Ghanekar, A. *et al.* Near-field thermal rectification devices using phase change periodic nanostructure. *Opt. Express* **26**, A209–A218. https://doi.org/10.1364/OE.26.00A209 (2018).
22. Castillo-López, S., Villarreal, C., Esquivel-Sirvent, R. & Pirruccio, G. Enhancing near-field radiative heat transfer by means of superconducting thin films. *Int. J. Heat Mass Transf.* **182**, 121922 (2022).
23. Castillo-López, S., Pirruccio, G., Villarreal, C. & Esquivel-Sirvent, R. Near-field radiative heat transfer between high-temperature superconductors. *Sci. Rep.* **10**, 16066 (2020).
24. Králík, T., Musilová, V., Fořt, T. & Srnka, A. Effect of superconductivity on near-field radiative heat transfer. *Phys. Rev. B* **95**, 060503 (2017).
25. Ge, L., Xu, Z., Cang, Y. & Gong, K. Modulation of near-field radiative heat transfer between graphene sheets by strain engineering. *Opt. Express* **27**, A1109–A1117. https://doi.org/10.1364/OE.27.0A1109 (2019).
26. Ghanekar, A., Ricci, M., Tian, Y., Gregory, O. & Zheng, Y. Strain-induced modulation of near-field radiative transfer. *Appl. Phys. Lett.* **112**, 241104. https://doi.org/10.1063/1.5037468 (2018).
27. Yu, R. & Fan, S. Time-modulated near-field radiative heat transfer. *Proc. Natl. Acad. Sci.* **121**, e2401514121 (2024).
28. Tian, Y. *et al.* A review of tunable wavelength selectivity of metamaterials in near-field and far-field radiative thermal transport. *Materials*https://doi.org/10.3390/ma11050862 *(2018).*
29. Kan, Y. *Metamaterials for Manipulation of Thermal Radiation and Photoluminescence in Near and Far Fields* (Springer Nature, 2022).

30. Liu, X. L., Bright, T. J. & Zhang, Z. M. Application conditions of effective medium theory in near-field radiative heat transfer between multilayered metamaterials. *J. Heat Transf.* **136**, 092703–092703 (2014).
31. Chang, J.-Y., Sabbaghi, P. & Wang, L. Near-field radiative heat transfer between nanowire-based dual uniaxial magneto-dielectric metamaterials. *Int. J. Heat Mass Transf.* **158**, 120023 (2020).
32. Biehs, S.-A., Ben-Abdallah, P., Rosa, F. S., Joulain, K. & Greffet, J.-J. Nanoscale heat flux between nanoporous materials. *Opt. Express* **19**, A1088–A1103 (2011).
33. Cui, G.-C., Zhou, C.-L., Zhang, Y. & Yi, H.-L. Near-field radiative heat transfer between nonpolar epsilon-near-zero dielectric-filled si gratings. *Phys. Rev. B* **109**, 125430 (2024).
34. Castillo-López, S. G., Esquivel-Sirvent, R., Villarreal, C. & Pirruccio, G. Near-field radiative heat transfer management by sub-wavelength plasmonic crystals. *Appl. Phys. Lett.* **121**, 201708. https://doi.org/10.1063/5.0123232 (2022).
35. Luo, M., Zhao, J., Liu, L. & Antezza, M. Radiative heat transfer and radiative thermal energy for two-dimensional nanoparticle ensembles. *Phys. Rev. B* **102**, 024203 (2020).
36. Ott, A. & Biehs, S.-A. Topological near-field heat flow in a honeycomb lattice. *Int. J. Heat Mass Transf.* **190**, 122796 (2022).
37. Reyes-Coronado, A. *et al.* Enhancement of light absorption by leaky modes in a random plasmonic metasurface. *J. Phys. Chem. C* **126**, 3163–3170 (2022).
38. Zeng, C. *et al.* Graphene-empowered dynamic metasurfaces and metadevices. *Opto-Electron. Adv.* **5**, 200098 (2022).
39. Christensen, T., Jauho, A.-P., Wubs, M. & Mortensen, N. A. Localized plasmons in graphene-coated nanospheres. *Phys. Rev. B* **91**, 125414 (2015).
40. Raad, S. H. & Atlasbaf, Z. Tunable optical meta-surface using graphene-coated spherical nanoparticles. *AIP Adv.* **9**, 075224 (2019).
41. Yang, B., Wu, T., Yang, Y. & Zhang, X. Tunable subwavelength strong absorption by graphene wrapped dielectric particles. *J. Opt.* **17**, 035002 (2015).
42. Deng, S. *et al.* Interfacial engineering of plasmonic nanoparticle metasurfaces. *Proc. Natl. Acad. Sci.* **119**, e2202621119 (2022).
43. Song, J. *et al.* Thermal routing via near-field radiative heat transfer. *Int. J. Heat Mass Transf.* **150**, 119346. https://doi.org/10.1016/j.ijheatmasstransfer.2020.119346 (2020).
44. Bian, X. *et al.* Fabrication of graphene-isolated-au-nanocrystal nanostructures for multimodal cell imaging and photothermal-enhanced chemotherapy. *Sci. Rep.* **4**, 6093 (2014).
45. Lu, W. *et al.* Bipolar carrier transfer channels in epitaxial graphene/sic core-shell heterojunction for efficient photocatalytic hydrogen evolution. *Adv. Mater.* **27**, 7986–7991 (2015).
46. Ren, Q., You, J. W. & Panoiu, N. C. Large enhancement of the effective second-order nonlinearity in graphene metasurfaces. *Phys. Rev. B* **99**, 205404. https://doi.org/10.1103/PhysRevB.99.205404 (2019).
47. Wang, X. *et al.* Plasmon hybridization induced by quasi bound state in the continuum of graphene metasurfaces oriented for high-accuracy polarization-insensitive two-dimensional sensors. *Chin. Opt. Lett.* **20**, 042201. https://doi.org/10.1364/COL.20.042201 (2022).
48. Liu, X. L. & Zhang, Z. M. Giant enhancement of nanoscale thermal radiation based on hyperbolic graphene plasmons. *Appl. Phys. Lett.* **107**, 143114. https://doi.org/10.1063/1.4932958 (2015).
49. Hu, Y., Li, H., Zhu, Y. & Yang, Y. Enhanced near-field radiative heat transport between graphene metasurfaces with symmetric nanopatterns. *Phys. Rev. Appl.* **14**, 044054. https://doi.org/10.1103/PhysRevApplied.14.044054 (2020).
50. Francoeur, M., Mengüç, M. P. & Vaillon, R. Spectral tuning of near-field radiative heat flux between two thin silicon carbide films. *J. Phys. D Appl. Phys.* **43**, 075501 (2010).
51. Hu, Y. *et al.* Enhanced near-field radiative heat transfer between core-shell nanoparticles through surface modes hybridization. *Fundam. Res.*https://doi.org/10.1016/j.fmre.2023.03.021 *(2023)*.
52. Falkovsky, L. A. Optical properties of graphene. *J. Phys. Conf. Ser.* **129**, 012004 (2008).
53. Nikbakht, M. Radiative heat transfer between core-shell nanoparticles. *J. Quant. Spectrosc. Radiat. Transf.* **221**, 164–171 (2018).
54. Tzarouchis, D. C. & Sihvola, A. General scattering characteristics of resonant core-shell spheres. *IEEE Trans. Antennas Propag.* **66**, 323–330. https://doi.org/10.1109/TAP.2017.2769688 (2018).
55. Campione, S., Brener, I. & Marquier, F. Theory of epsilon-near-zero modes in ultrathin films. *Phys. Rev. B* **91**, 121408. https://doi.org/10.1103/PhysRevB.91.121408 (2015).
56. Vassant, S., Hugonin, J.-P. & Greffet, J.-J. Quasi-confined enz mode in an anisotropic uniaxial thin slab. *Opt. Express* **27**, 12317–12335. https://doi.org/10.1364/OE.27.012317 (2019).
57. Liu, R. *et al.* Near-field radiative heat transfer in hyperbolic materials. *Int. J. Extrem. Manuf.* **4**, 032002 (2022).

Acknowledgements

S.G.C-L., S.C-L., and D.N.C-L. acknowledge financial support from UNAM DGAPA PAPIIT Grant No. TA100724. The authors acknowledge R. Esquivel-Sirvent for helpful discussions and comments and express gratitude to Carlos Ernesto López Natarén for helping with the high-performance computing infrastructure at Instituto de física, UNAM, where we run our calculations and his valuable support. S.C-L. acknowledges financial support from Tecnológico Nacional de México, Grant No. 15279.22-PD.

Author contributions

S.G.C-L. conducted the numerical calculations. S.G.C-L., S.C-L. and D.N.C-L. analyzed the results. All authors contributed to the manuscript.

Competing interests

The authors declare no competing interests.

Additional information

Supplementary Information The online version contains supplementary material available at https://doi.org/10.1038/s41598-024-69023-0.

Correspondence and requests for materials should be addressed to S.G.C.-L.